Characterizing T Cell Movement within Lymph Nodes in the Absence of Antigen[1]

Catherine Beauchemin, Narendra M. Dixit,[2] and Alan S. Perelson[3]

The recent application of two-photon microscopy to the visualization of T cell movement has presented trajectories of individual T cells within lymphoid organs both in the presence and in the absence of Ag-loaded dendritic cells. Remarkably, even though T cells largely move along conduits of the fibroblastic reticular cell network, they appear to execute random walks in lymphoid organs rather than chemotaxis. In this study, we analyze experimental trajectories of T cells using computer simulations of idealized random walks. Comparisons of simulations with experimental data provide estimates of key parameters that characterize T cell motion in vivo. For example, we find that the distance moved before turning is about twice the distance between intersections in the fibroblastic reticular cell network, suggesting that at an intersection a T cell will turn onto a new fiber ~50% of the time. Although the calibrated model appears to offer an accurate representation of T cell movement, it has also uncovered inconsistencies across different experimental data sets. *The Journal of Immunology,* **2007, 178: 5505–5512.**

Movement of T cells within lymphoid organs facilitates their interactions with other components of the immune system and enables transmission of information for immune surveillance and response. Often, as in the case of HIV infection, immune cell interactions also allow the spread of infection within an individual.

Two-photon microscopy has allowed the direct visualization of the movement of T cells within lymph nodes, giving new insights into immune interactions (1–4). From these experiments, the locations of individual T cells moving in lymphoid organs are obtained as a function of time (5–8). The instantaneous and mean velocities of T cells, their mean free paths, and their trajectories in the presence and the absence of Ag-presenting dendritic cells can thus be determined. Further, such experiments have revealed that T cells move by crawling along the strands of a fibroblastic reticular cell (FRC)[4] network (1). Remarkably, trajectories of individual T cells obtained from these studies suggest that T cell motion is random and not directed by chemokine gradients over large distances. The mean displacement of the T cells from their respective initial positions is found to increase linearly with the square root of time, indicative of the random-walk nature of T cell movement. Thus, even though T cell motion may be along conduits of the FRC network, by virtue of the dimensions of the network and its frequent crossing points, movement along the network appears to give rise to the seemingly random-walk nature of T cell motion (1).

This paper assembles and analyzes the available data and proposes a simple model for T cell movement. The simulations of the model capture observed T cell trajectories quantitatively and yield estimates of underlying parameters that characterize T cell motion in vivo. The resulting insights will be particularly useful given the growing interest in the development of spatial mathematical models for viral infections (9–15).

Describing T Cell Movement

Experimental data of the mean $2d$ T cell displacement vs $\sqrt{\text{time}}$ presented in Fig. 1 appears to display two distinct regimes. At small times, the displacement appears to have a quadratic dependence on $\sqrt{\text{time}}$ (i.e., linear dependence on time), which resembles what one would expect for a particle moving in a straight line at a fixed speed. In contrast, for larger times, the displacement appears to depend linearly on the square root of time, suggesting that the cells are diffusing. For times smaller than the time scale of a single step of a random walk, a particle performing that random walk will move in a straight line as it takes that step, yielding a quadratic shape at small times. For larger times, however, the consecutive steps taken by the particle in random directions yield a linear shape. This is illustrated in Fig. 2, and can be seen in Fig. 1 where we present data obtained from the works of Mempel et al. (5) and Miller et al. (6–8).

Although the manner in which T cells crawl is not fully understood, many characteristics are thought to be similar to the crawling of amebas of the lower eukaryote *Dictyostelium discoideum* (16). Migration is initiated when the T cell adopts a polarized (elongated) shape. This is followed by the formation of a lamellipodium at the leading edge and a uropod at the trailing edge (Ref. 17 and see Fig. 1 in Ref. 18). To move, the T cell anchors its uropod to the crawling surface, shifts all of its cytoplasm to the front, retracts the uropod, and starts another contraction-retraction cycle (see Fig. 1 in Ref. 19). Rather than moving in a fully unrestricted manner, Bajénoff et al. (1) recently showed that T cells traffic within lymph nodes by crawling along the network formed by the interconnected FRCs found in the paracortex region of lymph nodes.

Theoretical Biology and Biophysics, Los Alamos National Laboratory, Los Alamos, NM 87545

Received for publication November 13, 2006. Accepted for publication February 14, 2007.

The costs of publication of this article were defrayed in part by the payment of page charges. This article must therefore be hereby marked *advertisement* in accordance with 18 U.S.C. Section 1734 solely to indicate this fact.

[1] This work was performed under the auspices of the U.S. Department of Energy under Contract DE-AC52-06NA25396 and supported in part by Mathematics of Information Technology and Complex Systems (to C.B.), University of New Mexico/Los Alamos National Laboratory Joint Science and Technology Laboratory (to C.B.), and National Institutes of Health Grants R37-AI28433, R01-RR06555, and P01-AI071195 (to A.S.P.).

[2] Current address: Department of Chemical Engineering, Indian Institute of Science, Bangalore, India.

[3] Address correspondence and reprint requests to Dr. Alan S. Perelson, Los Alamos National Laboratory, MS K710, T-10, Los Alamos, NM 87545. E-mail address: asp@lanl.gov

[4] Abbreviations used in this paper: FCR, fibroblastic reticular cell; SSR, sum of the squared residuals.

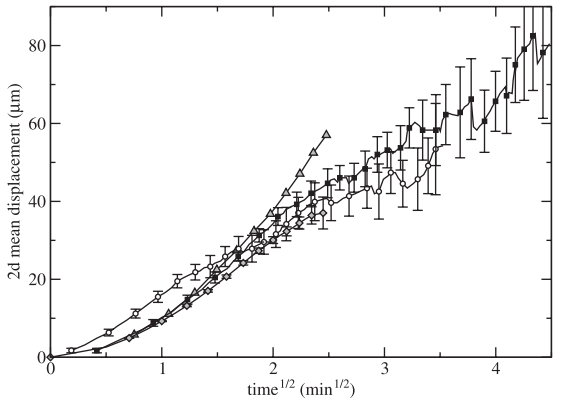

FIGURE 1. Two-dimensional ($2d$) mean displacement of T cells as a function of the square root of time from Miller et al. (8) (open circle), Miller et al. (7) (filled square), Miller et al. (6) (△), and from calculations based on individual T cell tracks used in Mempel et al. (5) (gray diamonds). SDs were reported only in Miller et al. (7, 8) and were computed from the tracks for Mempel et al. (5). Only a subset of data points is plotted for clarity.

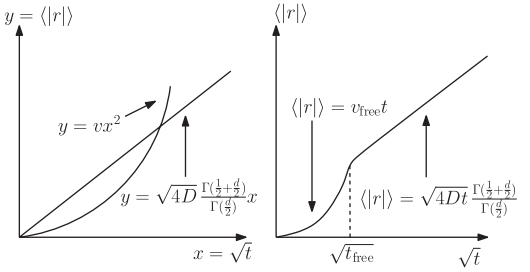

FIGURE 2. *Left,* The graph of the mean displacement, $\langle |r| \rangle$, as a function of the square root of time ($\sqrt{t}$) has a quadratic shape for motion in a straight line at fixed velocity, v, and a linear shape for a random walk or diffusion in d dimensions. *Right,* The results from T cell movement experiments are quadratic for small times and linear for larger times and thus resemble the curve on the right. The $\Gamma(1/2 + d/2)/\Gamma(d/2)$ term in the formulas results from using the mean displacement, $\langle |r| \rangle$, rather than the root mean squared displacement, $\sqrt{\langle r^2 \rangle}$, as a function of $\sqrt{\text{time}}$, as the y-axis (see *Materials and Methods*).

In our simulations, we adopt a minimalist description of T cell motion. We let a T cell perform an unhindered random walk (diffuse) with a mean free time t_{free}, during which the cell crawls in a straight line at a fixed speed v_{free}. At the end of each free run, we allow for a pause time, t_{pause}, during which the T cell is immobile as it reorganizes the cellular machinery, allowing it to turn. The cell then picks a new random direction, undergoes another free run, and so on. This scheme of movement is somewhat similar to the run-and-tumble motion of certain bacteria such as *Escherichia coli* (20), except that T cells reorient their lamellipodium, rather than tumble, between each free run. Averaging over the movement of many cells then allows us to determine the mean displacement of cells over time as a function of the parameters t_{free}, v_{free}, and t_{pause}. Comparison with experiments allows us to identify the key parameters characterizing this random walk.

Materials and Methods

Experimental data

The experimental data used to calibrate our model was taken from four different publications (5–8). These papers were chosen because they presented the mean displacement of T cells as a function of the square root of time, which we used to fit our T cell movement model. Dr. T. R. Mempel (CBR Institute for Medical Research, Harvard Medical School, Boston, MA) provided us with data containing the individual $CD8^+$ T cell tracks (t, x, y, z) from which we were able to compute the mean $2d$ displacement. To obtain the $2d$ mean displacement reported by Miller et al. (6–8), we digitized the graphs and extracted the data points using the software Engauge Digitizer (M. Mitchell, *Engauge Digitizer,* http://digitizer.sourceforge.net). The $2d$ mean displacements as a function of $\sqrt{\text{time}}$ for all four publications are presented in Fig. 1.

Theoretical expression for the mean displacement

The $\Gamma(1/2 + d/2)/\Gamma(d/2)$ term in the formulas of Fig. 2 results from the fact that Miller et al. (6–8) and Mempel et al. (5) chose to present the mean displacement, $\langle |r| \rangle$, rather than the root mean squared displacement, $\sqrt{\langle r^2 \rangle}$, as a function of $\sqrt{\text{time}}$, as their y-axis. Let r be the displacement of a particle at time t given that it started at the origin at time 0. If the particle is undergoing a random walk in d dimensions with diffusion coefficient D, then its mean squared displacement as a function of time is given by

$$\langle r^2 \rangle = 2dDt, \tag{1}$$

for t much larger than the time scale of a single time step (20). This equation is also valid for particles moving in d dimensions the motion of which has been projected to $\delta < d$ dimensions. In such a case, the mean squared displacement projected to δ dimensions is $\langle r^2 \rangle = 2\delta Dt$, provided that motion in the x, y, and z directions are statistically independent. Thus, we have

$$\langle r^2 \rangle_{2d} = \langle x^2 \rangle + \langle y^2 \rangle = 4Dt. \tag{2}$$

An expression analogous to the one presented in Equation 1 for $\langle r^2 \rangle$ can be derived for $\langle |r| \rangle$. At time t, the displacement in d dimensions of a particle that started at the origin at time 0 is given by

$$|r| = \sqrt{\sum_{i=1}^{d} x_i^2}. \tag{3}$$

Let us define

$$\alpha_i = \frac{x_i}{\sqrt{2Dt}}, \tag{4}$$

so that $x_i = \sqrt{2Dt}\ \alpha_i$, and

$$\langle x_i^2 \rangle = 2Dt\, \langle \alpha_i^2 \rangle. \tag{5}$$

Because x_i, the displacement of a diffusing particle in direction i, is a Gaussian random variable of mean $\langle x_i \rangle = 0$ and variance $\langle x_i^2 \rangle = 2Dt$, it follows that α_i is a Gaussian random variable of mean 0 and variance 1. The mean displacement in d dimensions at time t would then be given by

$$\langle |r| \rangle = \sqrt{2Dt} \left\langle \sqrt{\sum_{i=1}^{d} \alpha_i^2} \right\rangle = \sqrt{2Dt}\, \langle \sqrt{\beta} \rangle, \tag{6}$$

where $\beta = \Sigma_{i=1}^{\mathrm{d}}\ \alpha_i^2$. The sum of the squares of d Gaussian random variables of mean 0 and variance 1 is a χ^2-distributed random variable with d degrees of freedom (E. W. Weisstein, *Chi-Squared Distribution*; http://mathworld.wolfram.com/Chi-SquaredDistribution.html). The $\frac{1}{2}$th moment of a χ^2-distributed random variable β with d degrees of freedom is given by (E. W. Weisstein; http://mathworld.wolfram.com/Chi-SquaredDistribution.html).

$$\langle \sqrt{\beta} \rangle = \frac{\sqrt{2}\,\Gamma\left(\frac{1}{2}+\frac{d}{2}\right)}{\Gamma\left(\frac{d}{2}\right)}. \tag{7}$$

Substituting this back into Equation 6, we obtain

$$\langle |r| \rangle = \sqrt{4Dt}\ \frac{\Gamma\left(\frac{1}{2}+\frac{d}{2}\right)}{\Gamma\left(\frac{d}{2}\right)}. \tag{8}$$

the expression found in Fig. 2.

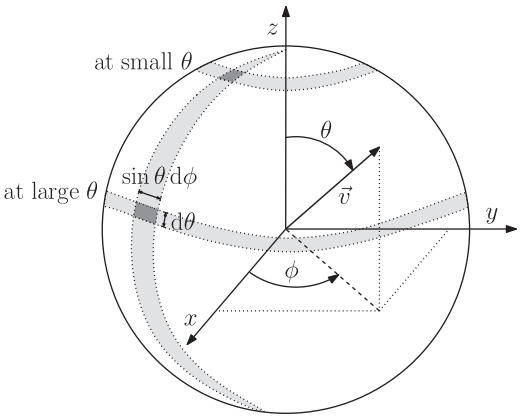

FIGURE 3. The angles of the velocity vector, $\vec{v}$, are defined such that θ is the angle measured southward from the positive z-axis, and ϕ is the angle measured eastward from the positive x-axis. Notice how the area elements $\sin\theta\, d\theta\, d\phi$ (dark gray) yield different areas for different values of θ.

Simulation of T cell movement

Two-photon microscopy experiments report either two-dimensional (2*d*) (6–8) or three-dimensional (3*d*) (5) coordinates of T cells in lymphoid organs as a function of time. Because the experimental resolution in 3*d* is lower than in 2*d*, 3*d* results can be misleading. Because 2*d* data provide an adequate representation for the mean displacement, we simulate the 3*d* motion of T cells projected onto 2*d* by using the standard relationship between cartesian and spherical coordinates. The algorithm we use is described below.

Let (x_t, y_t) be the 2*d* coordinates of a T cell at time t. At time $t + \Delta t$, the position of the particle is given by

$$x_{t+\Delta t} = x_t + \Delta t \cdot (|\vec{v}| \sin\theta \cos\phi) \tag{9}$$

$$y_{t+\Delta t} = y_t + \Delta t \cdot (|\vec{v}| \sin\theta \cos\phi) \tag{10}$$

where $|\vec{v}|$ is the magnitude of the 3*d* velocity of the T cell, and the angles θ and ϕ are as defined in Fig. 3. Thus $|\vec{v}| \sin\theta \cos\phi$ is the x-component of the T cell velocity used in Equation 9 above and $|\vec{v}| \sin\theta \sin\phi$ is the corresponding y-component used in Equation 10. Equations 9 and 10 thus allow us to simulate the 2*d* projection of the 3*d* movement of T cells without explicitly considering the z-component of motion.

To mimic the successive periods of running and pausing, we set $|\vec{v}|$ to v_{free} for a length of time t_{free}, then set it to zero for a length of time t_{pause}, and so on. At the beginning of each free run, i.e., when $|\vec{v}|$ is switched from zero to v_{free}, new values for θ and ϕ are picked at random. In order to distribute the chosen directions of $\vec{v}$ uniformly over the sphere, we choose a random ϕ uniformly distributed in $[0, 2\pi)$, and choose a random θ distributed in $[0, \pi)$ according to the probability density $P = \frac{1}{2}\sin\theta$. In this way, there is a constant density per unit area element $\sin\theta\, d\theta\, d\phi$ (Fig. 3). If θ were to be chosen evenly in $[0, \pi)$, the resulting set of velocity vectors would be more dense toward the poles.

Each T cell run lasts 20 min, and we chose a step size $\Delta t = 1$ s. To prevent artifacts, which would result from the synchronization of pause times across T cell runs, the time for the first pause in each T cell run is chosen at random, uniformly distributed in $[-t_{\text{pause}} + \Delta t, t_{\text{free}}]$ (Fig. 4). When this value is negative, the T cell is started in a paused mode at time $t = 0$, and the magnitude of the negative number indicates for how long before $t = 0$ the cell has been in that state.

The 2*d* displacement of the T cell from its initial position $(x_0, y_0) = (0, 0)$ is computed using

$$r_t = \sqrt{x_t^2 + y_t^2}, \tag{11}$$

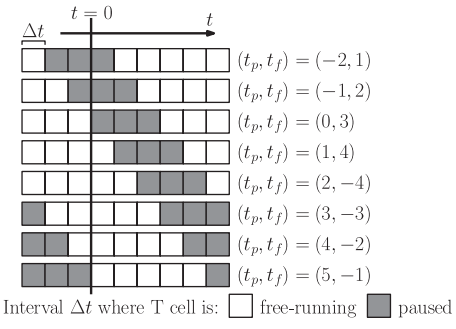

FIGURE 4. In each T cell run, the time for the first pause, t_p, which in turns sets the time of the first free run, t_f, is chosen at random uniformly over all possible choices, namely $[-t_{\text{pause}} + \Delta t, t_{\text{free}}]$. This is illustrated here for the case of $t_{\text{pause}} = 3$ time steps (the time interval during which a cell is paused) and $t_{\text{free}} = 5$ time steps (the time interval during which a cell in moving at constant speed v_{free}), where the duration of a time step is Δt.

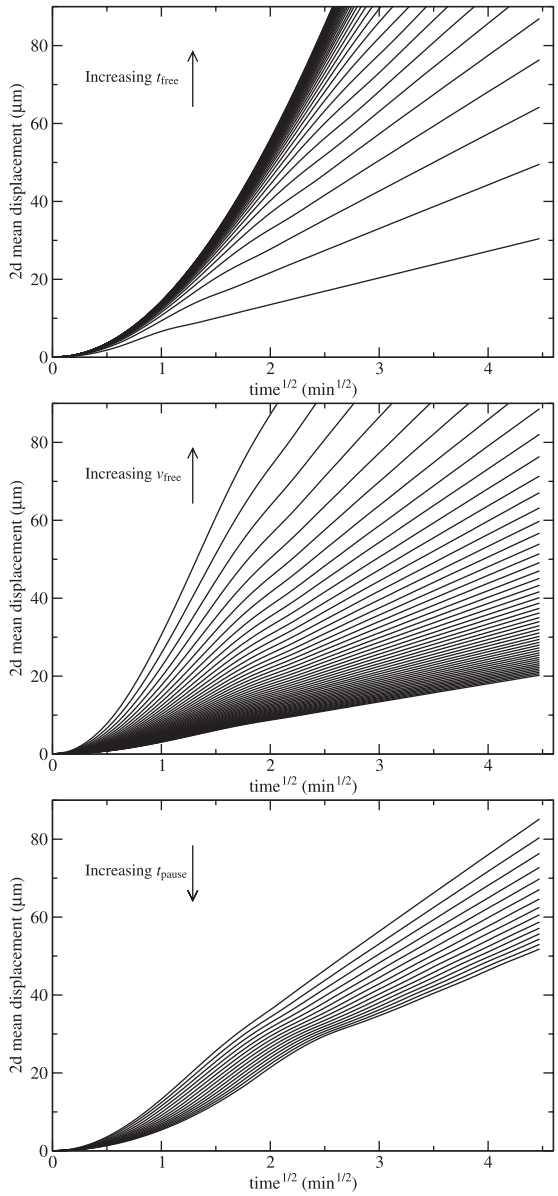

FIGURE 5. The effect of varying a single parameter at a time, while maintaining the other two parameters fixed, on the shape of the 2*d* mean displacement curve. When fixed, the parameters are set to $t_{\text{pause}} = 0.5$ min, $t_{\text{free}} = 2$ min, and $v_{\text{free}} = 18.8$ μm/min. Then, t_{free} is varied by increments of 0.5 min over the range [0.5, 20.0] min, $1/v_{\text{free}}$ rather than v_{free} is varied by increments of ~ 0.00367 min/μm over the range [0.02, 0.2] min/μm, and t_{pause} is varied by increments of 0.25 min over the range [0.0, 3.5] min. The simulation results were produced by averaging the individual displacement of 10^6 T cells for each triplet (t_{pause}, t_{free}, v_{free}).

for t from 0 to 20 min. We repeat the above procedure for $n = 10^6$ T cells and obtain the average displacement at time t,

$$\langle |r| \rangle = \frac{1}{N} \sum_{i=1}^{N} \sqrt{x_{t,i}^2 + y_{t,i}^2}, \tag{12}$$

where $(x_{t,i}, y_{t,i})$ is the position (x_t, y_t) of the ith T cell at time t.

Fig. 5 illustrates how each of the parameters t_{pause}, t_{free}, and v_{free} affects the $2d$ mean displacement as a function of the square root of time. The most important effect of increasing t_{free} is to increase of the slope of the curve at larger times, whereas that of increasing v_{free} is to generate a more pronounced curvature at smaller times. The effect of increasing t_{pause} is more subtle but is mostly a horizontal translation toward larger times of the time of transition between the quadratic and linear regimes of the $2d$ mean displacement.

To compare the T cell velocities in our model, $\vec{v}_{free}$, with those measured experimentally, namely the $2d$ velocities, $\bar{v}_{exp}$, the parameter v_{free} must be converted using

$$\bar{v}_{exp} = v_{free} \times \underbrace{\frac{\pi}{4}}_{3d \to 2d} \times \underbrace{\frac{t_{free}}{t_{free} + t_{pause}}}_{\text{actual} \to \text{measured}}. \tag{13}$$

The term $\pi/4$ is necessary to convert the $3d$ velocity of our simulation to its $2d$ equivalent for comparison with the velocities mentioned by Mempelet al. (5) and Miller et al. (6–8). It comes from the fact that $v_{2d} = v_{3d} \cdot \sin\theta$, where θ is as illustrated in Fig. 3. On average,

$$\langle \sin\theta \rangle = \int_0^{\pi} P(\theta) \sin\theta \, d\theta = \int_0^{\pi} \frac{\sin^2\theta}{2} \, d\theta = \frac{\pi}{4}. \tag{14}$$

The experimental instantaneous velocity, $\bar{v}_{exp}$, is computed from the distance traveled by a T cell in the xy-plane over a short time interval (~10 s) (5–8). Over this time interval, some T cells are paused, some T cells are moving, and some will experience both states sequentially. The term $t_{free}/(t_{free} + t_{pause})$ accounts for this fact and converts the velocity from our simulation to the T cell velocity that would be measured experimentally.

In light of recent experiments which showed that T cells move in lymph nodes by crawling along the FRC network (1), it is of interest to compare the persistence length or mean free path of the free runs of the T cells in our model to the mean distance between intersections in the FRC network. This distance is reported to range between 5 and 37 μm, with an average of $\sim 17 \pm 7$ μm for the six lymph nodes studied in Ref. 1. For this purpose, we introduce the variable d_{free} which is simply

$$d_{free} = t_{free} \times v_{free}. \tag{15}$$

Results

Comparison with experiments

For each value of the parameter triplet (t_{pause}, t_{free}, v_{free}), the individual trajectories of 10^6 T cells were simulated, varying only the time of the first pause and the seed of the random number generators, and the average of their $2d$ displacements was computed. This was repeated as parameter values were varied over the ranges $t_{pause} = [0, 3.5]$ min, $t_{free} = [0.5, 20]$ min, and $v_{free} = [5, 50]$ μm/min. Then, for each triplet value, we computed the sum of the squared residuals (SSR) between the simulation results and an experimental data set composed of all the experimental data from the four publications (5–8). The SSR were then used to rank triplet values from best to worst fit (Table I).

From Table I, we see that the triplet value of ($t_{pause} = 0.5$ min, $t_{free} = 2$ min, $v_{free} = 18.8$ μm/min) minimizes the SSR between the simulation results and the set composed of the combined experimental data. If, for simplicity, one only considers fits for which there is no pause time between free runs ($t_{pause} = 0$), the doublet value of ($t_{free} = 2$ min, $v_{free} = 16.6$ μm/min), i.e., the 6th best-fitting triplet, minimizes the SSR between the simulation results and the data of the combined sets. Also, the experimental velocity, $\bar{v}_{exp}$, obtained from the best-fitting triplet values compare well with the reported experimental T cell velocity of ~11 μm/min (5–8).

Table I. *Best triplets for the set of combined data*

Rank[a]	t_{pause} (min)	t_{free} (min)	v_{free} (μm/min)	$\bar{v}_{exp}$[b] (μm/min)	d_{free}[c] (μm)	SSR (μm^2/min)
1st	0.50	2.0	18.8	11.8	38	3387
2nd	0.50	2.5	16.6	10.8	41	3422
3rd	0.25	2.0	17.6	12.3	35	3455
4th	1.25	1.5	26.1	11.2	39	3488
5th	0.75	1.5	23.8	12.5	36	3494
6th	0.00	2.0	16.6	13.0	33	3503
7th	0.00	3.0	14.0	11.0	42	3513
8th	1.00	2.0	20.2	10.6	40	3526
9th	1.50	2.0	21.9	9.8	44	3550
10th	0.50	1.5	21.9	12.9	33	3559

[a] The set of combined data consists of the experimental data from all four publications (5–8). The parameter t_{pause} was varied from 0 to 3.5 min, t_{free} from 0.5 to 20 min, and v_{free} from 5 to 50 μm/min. The triplets (t_{pause}, t_{free}, v_{free}) have been sorted in order of increasing sum of squared residuals, SSR, between the experimental data and the simulation results. The simulation results were produced by averaging the individual displacement of 10^6 T cells for each parameter triplet.
[b] Computed using Equation 13.
[c] Computed using Equation 15.

Table I also shows the mean free path length, d_{free}, for each triplet. This distance for the best-fitting triplets is about twice the distance between intersections in the FRC network, which average $\sim 17 \pm 7$ μm (1). This suggests that at an intersection, ~50% of the time a T cell will turn onto a new fiber and ~50% of the time the T cell will continue along its original fiber. To see this, assume that the distance between intersections in the FRC network is L, and that a cell has probability p of continuing along the same fiber at an intersection. A T cell has a probability $(1 - p)$ of going straight for only a distance L and then turning at the first intersection, a probability $p(1 - p)$ to go straight for a distance $2L$ by going straight through the first intersection and then turning at the next, a probability $p^2(1 - p)$ to go straight for a distance $3L$ by going straight through the first two intersections and turning at the third, etc. Thus, we can express the average distance traveled by a T cell without branching as

$$\begin{aligned} d_{free} &= L(1-p) + 2Lp(1-p) + 3Lp^2(1-p) + \cdots \\ &= L(1-p) \sum_{N=1}^{\infty} N p^{N-1} \\ &= \frac{L}{(1-p)} \text{ for } |p| < 1, \end{aligned} \tag{16}$$

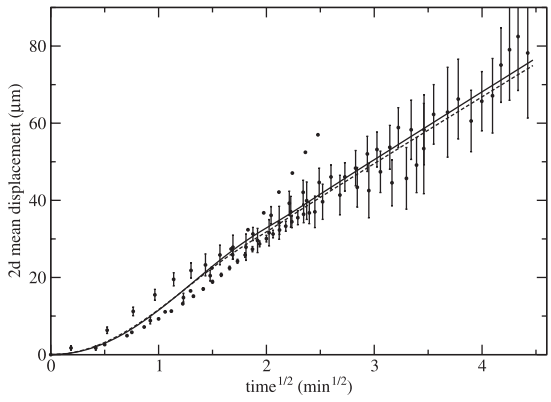

FIGURE 6. The combined experimental data from Mempel et al. (5) and Miller et al. (6–8) (●) along with the best-fitting triplet ($t_{pause} = 0.5$ min, $t_{free} = 2$ min, $v_{free} = 18.8$ μm/min) (——), and the best-fitting doublet or 6th best-fitting triplet ($t_{pause} = 0$, $t_{free} = 2$ min, $v_{free} = 16.6$ μm/min) (----). The simulation results were produced by averaging the individual displacement of 10^6 T cells for each triplet (t_{pause}, t_{free}, v_{free}).

such that for $p = 1/2$, the average distance traveled without branching is $2L$, or double the mean distance between intersections.

In the end, there is not much difference between the set of combined experimental data and the simulations obtained with the best-fitting doublet or triplet (Fig. 6). Thus, given the limited amount of available experimental data, it is not possible to narrow the range of acceptable values any further or to infer the length or even the existence of a pause time between successive free runs.

The best-fitting triplet and doublet found here should not be regarded as the only solution, i.e., the parameter values that best characterize the motion of T cells in vivo in the absence of Ag. The sixth best-fitting triplet ($t_{pause} = 0$, $t_{free} = 2$ min, $v_{free} = 16.6$ μm/min), for example, has different parameter values from that of the best-fitting triplet but does not have a significantly worse SSR (3502 μm^2 vs 3387 μm^2, a 3% difference). To help in understanding where the best-fitting triplets are located with respect to one another in the parameter space of the model, Fig. 7 presents contour plots of the SSR across the parameter space of the triplets for the set of combined experimental data.

From Fig. 7, one can see that the best-fitting triplets appear to occupy a small volume in the parameter space, represented by the white areas on the graphs. Larger quantities of more precise experimental data would be necessary to reduce these areas and constrain the uncertainty on the parameters of the model.

Experimental discrepancies

In the previous section, a fit to a set composed of the combined experimental data from four different publications (5–8) was presented. Inspection of Fig. 1, however, reveals discrepancies between the various data sets which use different experimental procedures. For example, data from Miller et al. (8), which tracked both $CD4^+$ and $CD8^+$ T cells in mouse explanted cervical and inguinal lymph nodes, is not as curved as the other data at small times, and data from Miller

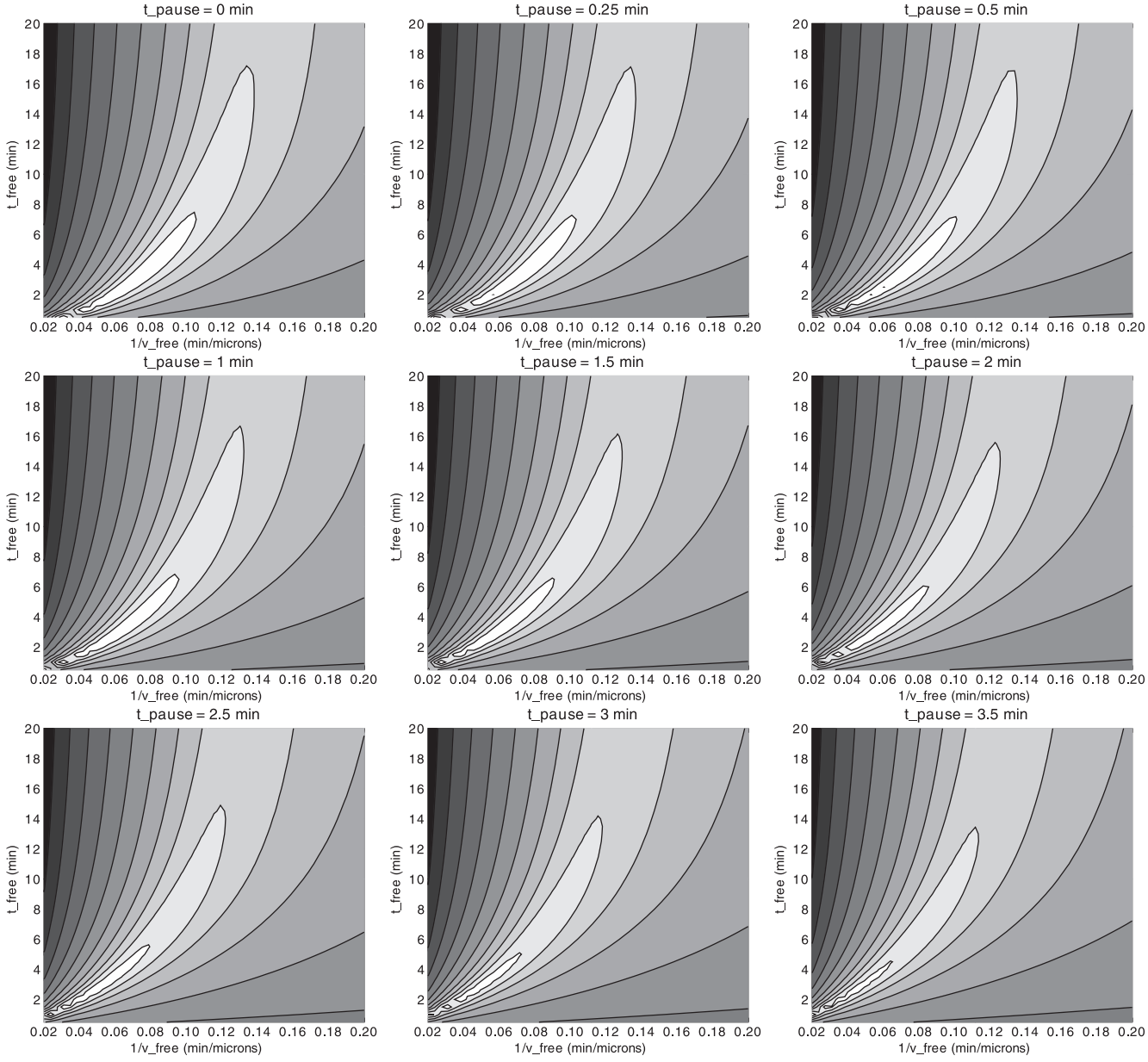

FIGURE 7. Contour plots presenting the natural logarithm of the SSRs, ln(SSR), between the simulation and the data set comprised of the combined experimental data from Mempel et al. (5) and Miller et al. (6–8) as a function of $1/v_{free}$ and t_{free} for various values of t_{pause}. Lighter shades of gray represent smaller SSR (better fits). Words following _ in the figure are subscripted in the text.

et al. (6), which tracked $CD4^+$ T cells in explanted cervical and inguinal lymph nodes of asphyxiated mice, appears to continue to exhibit a quadratic dependence of the mean displacement on the square root of time when the other data have entered the linear regime. To quantitatively explore these discrepancies, we computed the SSR between the simulation results and each experimental set individually over the full parameter space of the triplets explored above (Table II). For comparison purposes, Table II also presents how the best-fitting doublet and triplet found for the combined data sets fit each experimental data set individually. Fig. 8 presents the best-fitting triplet for each set along with the best-fitting doublet and triplet for the combined set against each experimental set.

The best-fitting triplets for the data of Miller et al. (8) differ from the best-fitting triplets of the combined sets in their smaller t_{free} and larger v_{free} values. This discrepancy is illustrated in Fig. 8 where the $2d$ mean displacement for the data of Miller et al. (8) has a more pronounced curve at smaller times and a less pronounced slope at larger times when compared with the combined set. This suggests that according to our model, the cells in the work of Miller et al. (8) are taking shorter steps, changing direction more often, and moving faster during steps. This is echoed by the smaller mean free paths, d_{free}, of the five best-fitting triplets which are in the range of 21–26 μm.

The best-fitting triplets for Miller et al. (7) differ most notably from the best-fitting triplets of the combined sets in their larger t_{pause} value. This discrepancy is illustrated in Fig. 8 where the $2d$ mean displacement for Miller et al. (7) appears to make the transition between the quadratic to the linear regime at larger times when compared with the combined set. According to our model, this would mean that the T cells in Miller et al. (7) pause for longer times between runs. The Miller et al. (7) triplets are most consistent with the best-fitting triplets of the combined sets because Miller et al. (7) contributed the largest number of data points to the combined sets and, in particular, was the only contributor of points for longer times ($\sqrt{t} < 3.5\ \sqrt{\text{min}}$), it therefore had a significant effect on the slope of the linear regime of the best-fitting triplets for the combined sets.

The discrepancy between the Miller et al. (6) $2d$ mean displacement and the other data sets is the most striking. Not surprisingly, the best-fitting triplets for Miller et al. (6) differ most significantly from the best-fitting triplets of the combined sets in their larger t_{free} values. This is illustrated in Fig. 8 where the $2d$ mean displacement for Miller et al. (6) seems to remain in the quadratic regime over the full length of the observation time (~6.25 min). According to our model, this would mean that in Miller et al. (6), T cells were moving in a straight line over the entire course of the experiment, i.e., for much longer than 6 min, at $3d$ speeds of ~13 μm/min. This is also echoed in the unrealistically large mean free paths, d_{free}, of the best-fitting triplets.

Finally, the best-fitting triplets for Mempel et al. (5) differ slightly from the best-fitting triplets of the combined sets in their larger t_{pause} and t_{free} and smaller v_{free} values. This is illustrated in Fig. 8 where these discrepancies translate to a smaller $2d$ mean displacement over time compared with the other data sets. Closer examination of the Mempel et al. (5) data reveals that the $2d$ mean displacement appears to plateau toward the end of the experiment (~6.25 min), suggesting that cells may be stopping or getting trapped after runs of this duration. The trajectory of any cell can be tracked for only as long as the cell remains in the imaging field. This introduces a bias whereby only cells with a trajectory that is confined to the imaging field for 6.25 min contribute to the mean displacement at that time. It is possible that such cells have motilities that differ from those of the other cells which have left the imaging field, and their exclusive contribution to the mean displacement at larger times would bias this value.

The experimental data from Miller et al. (6) and Mempel et al. (5) have the smallest SSR, whereas those of Miller et al. (7, 8) give worse SSR by about two orders of magnitude. This is due to the fact that the experimental data from the former two is quite smooth whereas that from the latter two is noisier, and thus harder to fit. In addition, it is important to consider that the experimental procedures differed among the four experiments. Miller et al. (8) considered $CD3^+$ T cells (both $CD4^+$ and $CD8^+$ T cells) and conducted the experiments in mouse explanted cervical and inguinal lymph nodes. In the data of Miller et al. (7), only $CD4^+$ T cells were considered, and the experiment was conducted in the inguinal lymph node of anesthetized mice. In Miller et al. (6), $CD4^+$ T cells were considered, but the mice were killed by CO_2 asphyxiation, and cervical or inguinal lymph nodes were explanted and maintained at 36°C under superfused medium bubbled with 95% O_2 and 5% CO_2. Finally, according to Mempel et al. (5), $CD8^+$ T cells were considered, and the experiments were conducted in the popliteal lymph nodes of anesthetized mice.

These differences in the experimental procedures could possibly account for the differences seen between the four data sets. Explanted lymph nodes are maintained at 36°C under superfused medium bubbled with 95% O_2 and 5% CO_2 to take account of the fact that the lymphoid environment is thought to operate at a relatively low oxygen tension (2). But despite these precautions, it remains

Table II. *Best triplets for each experimental data set*

Rank[a]	t_{pause} (min)	t_{free} (min)	v_{free} (μm/min)	$\bar{v}_{exp}$[b] (μm/min)	d_{free}[c] (μm)	SSR (μm^2/min)
Miller et al. (8)						
1st	0.50	0.5	42.2	16.6	21	337.6
2nd	0.25	0.5	36.6	19.1	18	341.6
3rd	0.25	1.0	23.8	14.9	24	449.3
4th	0.50	1.0	26.1	13.6	26	452.5
5th	0.00	1.0	21.9	17.2	22	463.9
55th	0.00	2.0	16.6	13.0	33	1135
109th	0.50	2.0	18.8	11.8	38	1469
Miller et al. (7)						
1st	2.50	1.5	32.2	9.5	48	805
2nd	1.75	2.5	20.2	9.4	51	830.8
3rd	1.25	2.5	18.8	9.9	47	844.7
4th	1.25	2.0	21.9	10.6	44	856.2
5th	1.75	2.0	23.8	10.0	48	861.5
47th	0.50	2.0	18.8	11.8	38	1082
133rd	0.00	2.0	16.6	13.0	33	1505
Miller et al. (6)						
1st	0.75	14.5	13.3	9.9	193	1.132
2nd	0.75	14.0	13.3	9.9	186	1.151
3rd	0.00	18.5	12.7	10.0	235	1.212
4th	1.00	15.5	13.3	9.8	206	1.223
5th	0.50	13.0	13.3	10.1	173	1.234
4374th	0.50	2.0	18.8	11.8	38	617.2
4745th	0.00	2.0	16.6	13.0	33	713.4
Mempel et al. (5)						
1st	0.50	3.0	14.0	9.4	42	1.776
2nd	1.50	2.5	17.6	8.7	44	3.199
3rd	0.25	3.5	12.7	9.3	44	3.268
4th	1.00	2.5	16.6	9.3	41	5.319
5th	1.00	3.0	14.8	8.7	44	5.379
1492nd	0.00	2.0	16.6	13.0	33	149.7
2380th	0.50	2.0	18.8	11.8	38	219.2

[a] The parameter t_{pause} was varied from 0 to 3.5 min, t_{free} from 0.5 to 20 min, and v_{free} from 5 to 50 μm/min. The triplets (t_{pause}, t_{free}, v_{free}) have been sorted in order of increasing SSRs between the data and the simulation results. The simulation results were produced by averaging the individual displacement of 10^6 T cells for each parameter triplet. The fit to each individual data set of the best-fitting doublet and triplet for the combined data sets (see Table I) is also presented.

[b] Computed using Equation 13.

[c] Computed using Equation 15.

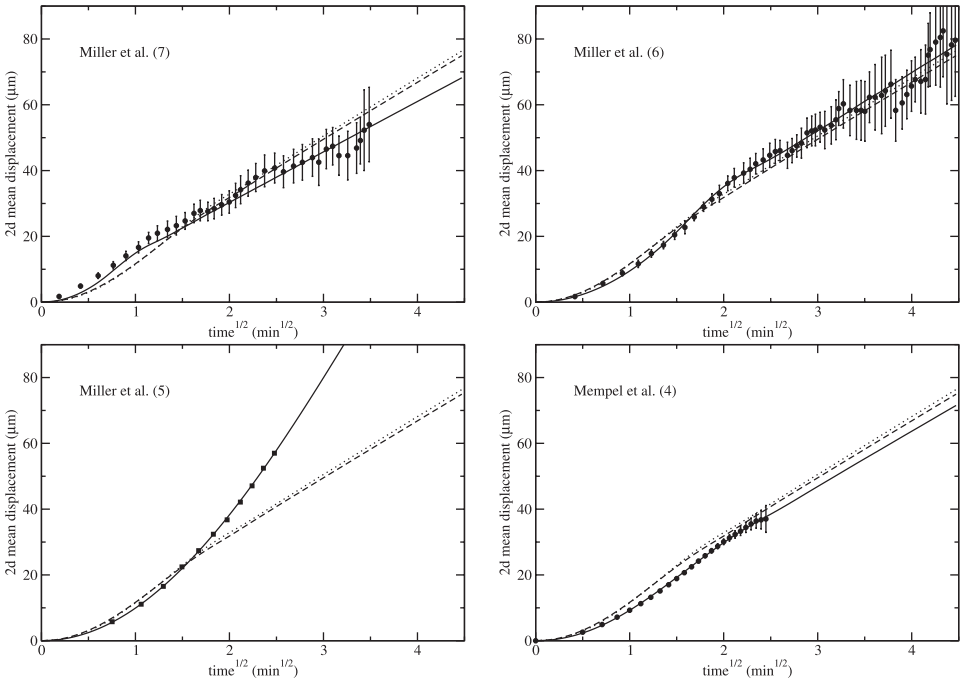

FIGURE 8. The individual experimental data from Mempel et al. (5) and Miller et al. (6–8) (●) along with their respective best-fitting triplet (——), the best-fitting triplet to the combined data (t_{pause} = 0.5 min, t_{free} = 2 min, v_{free} = 18.8 μm/min) (···), and the best-fitting doublet to the combined data (t_{free} = 2 min, v_{free} = 16.6 μm/min) (– – – –). The simulation results were produced by averaging the individual displacement of 10^6 T cells for each triplet (t_{pause}, t_{free}, v_{free}).

that explanted lymph nodes are deprived of their normal blood and lymphatic circulations, and this might have an effect on the experimental results obtained (2, 3). Additionally, the four experiments were conducted using a variety of lymph nodes (e.g., popliteal, cervical, inguinal). Differences in the underlying structures of different lymph nodes such as the density of dendritic cells (4), or more importantly the differences in the structure of the FRC network along which the T cells crawl (1), which could differ between lymph nodes in different anatomical locations or depend on the genetic background, sex, or age of the experimental animal, could explain the differences seen in the motility patterns among the four experiments.

Overall, the experimental data do not differ too significantly from the fit to the combined data set, except for Miller et al. (6), and the model does appear to provide a fair description of T cell movements in lymph nodes.

Discussion

From the data obtained by two-photon microscopy, the motion of T cells appears to be consistent with the cells performing a random walk for displacements over long times and following straight trajectories over short periods of times. Consequently, we proposed a simple model for the motion of T cells in lymph nodes in the absence of Ag in which T cells move in a straight line at fixed velocity v_{free} for a time t_{free}, pause for a time t_{pause} to reposition their lamellipods and uropod as they randomly pick a new direction to move in, and so on. We have found that this simple model appears to give results that agree best with experimental results for t_{pause} = 0.5 min, t_{free} = 2 min, and v_{free} = 18.8 μm/min.

If, for simplicity, one only considers fits to the experimental data for which there is no pause time between free runs (t_{pause} = 0), picking t_{free} = 2 min, and v_{free} = 16.6 μm/min yields best agreement between the simulation results and the data. Overall, the addition of a pause time to the model does not significantly improve the agreement between the experimental data and the simulation results and as such is not absolutely necessary.

It is important that the pause time, which we have added to account for the physiological time necessary for a T cell to turn, should not alternatively be interpreted as the time for contact between a T cell and a dendritic cell. The pause time for our best fit was t_{pause} = 30 s, whereas dendritic cell-T cell contacts, in the absence of Ag, are consistently reported to last ~3 min (5, 6, 21).

It is also important to place our model in the context of the results of Bajénoff et al. (1) that showed T cells traffic within lymph nodes by crawling along a network of "roads" formed by interconnected FRCs. We compared the mean free paths, $d_{free} = t_{free} \times v_{free}$, computed from the best-fitting triplets to the mean distance between intersections in the FRC network. The mean free paths of 38 μm found for the best-fitting triplet and 33 μm found for the best-fitting doublet are about twice the distance between intersections in the FRC network, which averages 17 ± 7 μm (1). This suggests that at an intersection, ~50% of the time a T cell will turn onto a new fiber and ~50% of the time the T cell will continue along its original fiber. This is an interesting prediction, which should be easily verifiable.

In our model, the angles ϕ and θ are picked randomly at the beginning of each free run for each T cell. In contrast, cells traveling along the FRC strands would, at each intersection, have a choice between a restricted set of angles corresponding to the orientation of the strands available at that intersection. There is no information available regarding the angles available to the T cells at FRC strand intersections. One could, however, imagine that by picking angles at random, we are in fact picking the topology of the network onto which the T cells are crawling. The fact that subsequent T cells would pick different angles would simply mean that they have chosen a different path within the network. As more information about the topology of the FRC network becomes available, it will be possible to refine the choice of angles in our model to account for the new information.

Our model was created to be simple and efficient so as to support large-scale simulations of whole lymph nodes. For this reason, a number of simplifications were made. For instance, a fixed velocity of v_{free} is assigned to all of the 10^6 T cells simulated. In reality, the population of T cells exhibit a range of velocities with distributions as shown in Fig. 2*C* in Ref. 8 and Fig. 3*D* in Ref. 7. We have modified our simulations to explore the effect of having variable velocities across the T cell population. In the modified simulations, each of the 10^6 T cells was assigned a different velocity for the duration of the run. The velocities assigned to each T cell

were picked randomly from a Gaussian distribution of mean v_{free} with a SD of 5 μm/min. The deviation was picked so as to resemble the distributions shown in Fig. 2*C* in the 2002 work of Miller et al. (8) and Fig. 3*D* in the 2003 work of Miller et al. (7). We found that sample simulations where T cell velocities were picked randomly from this Gaussian distribution yielded mean displacement vs $\sqrt{\text{time}}$ curves that were indistinguishable from those produced by the model described in the paper where all T cells were assigned the same velocity.

Although our model does not explicitly consider the FRC network, simplifies the range of velocities exhibited by T cells to a single fixed velocity, and allows a random angle to be picked before each free run rather than restrict angles according, for example, to the physiology of the FRC network, it still agrees well with the experimental data for the mean displacement and mean velocity of the T cells (5–8). This is advantageous for spatial mathematical modelers because this makes modeling T cell movement simple and efficient.

These results do not exclude the possibility that chemokine attractants may direct the motion of T cells. The possibility of a chemokine gradient guiding the movement of T cells has been considered by A. K. Chakraborty (personal communication), who showed that one can observe random walk behavior in the presence of chemokine gradients as long as their effect was sufficiently short-ranged.

A more detailed model for lymphocyte movement has been proposed by Meyer-Hermann and Maini (22) and compared against B and T cell movement data from Miller et al. (8). Their model is a modified 2*d* cellular automaton-type Potts model (23, 24), where a cell is represented by a collection of subunits that are the lattice sites occupied by the cell volume. Like ours, their model also suggests a run-and-pause dynamics but implements it in more detail, integrating intracellular dynamics in a generic way. The subunits that make up a cell are moved individually in the direction chosen for active movement under constraints to maintain constant cell volume. After a period of movement, the cell undergoes reshaping and the subunits are moved so as to return the cell shape to a sphere. Interestingly, like ours, the mean displacement vs $\sqrt{\text{time}}$ produced by their model also disagrees with that of Miller et al. (8) at early times. In addition to the mean displacement, this model also yields a distribution of lymphocytes velocities that compares well with the spread seen in vivo.

Another detailed model for the movement of T cells and dendritic cells in lymph nodes was proposed by Beltman et al. (25). They use it to investigate the possibility that T cells and dendritic cells owe the characteristics of their motility patterns (i.e., run-and-pause random walk) to the anatomical structure of lymph nodes. Like the Meyer-Hermann and Maini model, theirs is a Potts model, where each cell is represented by a collection of neighboring sites, but it is a 3*d* rather than a 2*d* model. Using this model, the authors demonstrate that the run-and-pause random walk nature of T cell and dendritic cell motility need not be an intrinsic characteristic of cell motility. Rather, these characteristics emerge as a consequence of the anatomical barriers encountered by the cells which give rise to velocity fluctuations and mean displacements that are in good agreement with experimental data.

Although these models better describe lymphocyte movement by integrating more details, they are more computer intensive than ours for equivalent mean displacement results and may not lend themselves well to large scale simulations of, for example, whole lymph nodes.

In conclusion, we have proposed a simple description of T cell movement that matches experimental data and that can be implemented in a simple and computationally efficient manner.

Acknowledgments

We thank Dr. Thorsten R. Mempel for providing the T cell trajectories used in Ref. 5 and Joost Beltman for helpful discussions. We also thank one of the referees for suggesting that we calculate d_{free} and compare it with the results in Ref. 1.

Disclosures

The authors have no financial conflict of interest.

References

1. Bajénoff, M., J. G. Egen, L. Y. Koo, J. P. Laugier, F. Brau, N. Glaichenhaus, and R. N. Germain. 2006. Stromal cell networks regulate lymphocyte entry, migration, and territoriality in lymph nodes. *Immunity* 25: 989–1001.
2. Cahalan, M. D., I. Parker, S. H. Wei, and M. J. Miller. 2002. Two-photon tissue imaging: seeing the immune system in a fresh light. *Nat. Rev. Immunol.* 2: 872–880.
3. Cahalan, M. D., and I. Parker. 2005. Close encounters of the first and second kind: T-DC and T-B interactions in the lymph node. *Semin. Immunol.* 17: 442–451.
4. Germain, R. N., F. Castellino, M. Chieppa, J. G. Egen, A. Y. Huang, L. Y. Koo, and H. Qi. 2005. An extended vision for dynamic high-resolution intravital immune imaging. *Semin. Immunol.* 17: 431–441.
5. Mempel, T. R., S. E. Henrickson, and U. H. von Adrian. 2004. T-cell priming by dendritic cells in lymph nodes occurs in three distinct phases. *Nature* 427: 154–159.
6. Miller, M. J., O. Safrina, I. Parker, and M. D. Cahalan. 2004. Imaging the single cell dynamics of $CD4^+$ T cell activation by dendritic cells in lymph nodes. *J. Exp. Med.* 200: 847–856.
7. Miller, M. J., S. H. Wei, M. D. Cahalan, and I. Parker. 2003. Autonomous T cell trafficking examined in vivo with intravital two-photon microscopy. *Proc. Natl. Acad. Sci. USA* 100: 2604–2609.
8. Miller, M. J., S. H. Wei, I. Parker, and M. D. Cahalan. 2002. Two-photon imaging of lymphocyte motility and antigen response in intact lymph node. *Science* 296: 1869–1873.
9. Beauchemin, C. 2006. Probing the effects of the well-mixed assumption on viral infection dynamics. *J. Theor. Biol.* 242: 464–477.
10. Beauchemin, C., J. Samuel, and J. Tuszynski. 2005. A simple cellular automaton model for influenza A viral infections. *J. Theor. Biol.* 232: 223–234.
11. Bezzi, M., F. Celada, S. Ruffo, and P. E. Seiden. 1997. The transition between immune and disease states in a cellular automaton model of clonal immune response. *Physica A* 245: 145–163.
12. Durrett, R. 1994. The importance of being discrete (and spatial). *Theor. Popul. Biol.* 46: 363–394.
13. Funk, G. A., V. A. Jansen, S. Bonhoeffer, and T. Killingback. 2005. Spatial models of virus-immune dynamics. *J. Theor. Biol.* 233: 221–236.
14. Strain, M. C., D. D. Richman, J. K. Wong, and H. Levine. 2002. Spatiotemporal dynamics of HIV propagation. *J. Theor. Biol.* 218: 85–96.
15. Zorzenon dos Santos, R. M. and S. Coutinho. 2001. Dynamics of HIV infection: a cellular automata approach. *Phys. Rev. Lett.* 87.
16. Friedl, P., S. Borgmann, and E.-B. Bröcker. 2001. Amoeboid leukocyte crawling through extracellular matrix: lessons from the *Dictyostelium* paradigm of cell movement. *J. Leukocyte Biol.* 70: 491–509.
17. Sànchez-Madrid, F., and M. A. del Pozo. 1999. Leukocyte polarization in cell migration and immune interactions. *EMBO J.* 18: 501–511.
18. Friedl, P., K. S. Zänker, and E.-B. Bröcker. 1998. Cell migration strategies in 3-D extracellular matrix: differences in morphology, cell matrix interactions, and integrin function. *Microsc. Res. Tech.* 43: 369–378.
19. Rydgren, L., B. Norberg, C. Håkansson, C. von Mecklenburg, and N. Söderström. 1976. Lymphocyte locomotion, I: the initiation, velocity, pattern, and path of locomotion in vitro. *Lymphology* 9: 89–96.
20. Berg, H. C. 1983. *Random Walks in Biology.* Princeton University Press, Princeton, pp. 6–12.
21. Miller, M. J., A. S. Hejazi, S. H. Wei, M. D. Cahalan, and I. Parker. 2004. T cell repertoire scanning is promoted by dynamic dendritic cell behavior and random T cell motility in the lymph node. *Proc. Natl. Acad. Sci. USA* 101: 998–1003.
22. Meyer-Hermann, M. E., and P. K. Maini. 2005. Interpreting two-photon imaging data of lymphocyte motility. *Phys. Rev. E* 71: 061912.
23. Graner, F., and J. A. Glazier. 1992. Simulation of biological cell sorting using a two-dimensional extended Potts model. *Phys. Rev. Lett.* 69: 2013–2016.
24. Glazier, J. A., and F. Graner. 1993. Simulation of the differential adhesion driven rearrangement of biological cells. *Phys. Rev. E* 47: 2128–2154.
25. Beltman, J. B., A. F. M. Marée, J. N. Lynch, M. J. Miller, and R. J. de Boer. 2007. Lymph node topology dictates T cell migration behavior. *J. Exp. Med.* In press.